

Amplitude and phase of shaped nonlinear excitation fields in a four-wave mixing microscope

Varun Raghunathan, Alexei Nikolaenko, Chao-Yu Chung, and Eric O. Potma^{a)}
 Chemistry Department and Beckmann Laser Institute, University of California Irvine, Irvine,
 California 92627, USA

(Received 30 August 2011; accepted 11 October 2011; published online 28 October 2011)

We describe precise measurements of the amplitude and phase profiles of tightly focused nonlinear excitation fields in a four-wave mixing (FWM) microscope. By combining spatial light modulator based beam shaping with interferometric detection, we present the focal FWM excitation fields of various Hermite-Gaussian and Laguerre-Gaussian LG₀₁ beam modes. We observe well-defined spatial phase patterns for the focal fields associated with these beam modes. Such precise measurements of shaped nonlinear excitation fields have implications for the development of resolution enhancement schemes and tip-enhanced imaging methods in FWM microscopy. © 2011 American Institute of Physics. [doi:10.1063/1.3657148]

The use of tightly focused laser spots in optical microscopy makes it possible to conduct precise optical measurements with sub-micrometer precision. Further control of the focal fields can be attained by shaping the phase of the incident field, producing focal volumes of alternate amplitude and phase profiles. This control of the focal field characteristics has enabled enhanced manipulation of the light-matter interactions in focus. For instance, the improved imaging resolution in stimulated emission depletion microscopy techniques,¹ the realization of excitations with a well-defined orbital angular momentum of light,² and the enhanced excitation of plasmonic tips with longitudinal polarization are all based on advanced phase-shaped focal fields.³

A unique opportunity arises when phase shaped excitation beams are employed in four-wave mixing (FWM) microscopy. Being a coherent technique, the signal is highly dependent on both the amplitude and phase of the focal excitation volume of a high-numerical aperture (NA) objective lens, offering a variety of manipulation techniques to control the radiation emanating from focus. Examples include selective imaging of interfaces^{4,5} and imaging with improved contrast and resolution.^{6–9}

For such advanced applications, it is important to have precise control over the amplitude and phase of the effective FWM excitation field. It is, therefore, desirable to accurately measure the complex excitation field at the FWM wavelength. Measuring the amplitude and phase of diffraction-limited focal volumes is, however, not straightforward. In the linear domain, there have been few demonstrations of complex focal field mapping by using interferometric detection of linear scattering from gold nanoparticles,¹⁰ by using fiber tips to probe near fields,¹¹ by using digital holography microscopy¹² or by measuring the spatial correlation of fluorescence emission.¹³ In this work, we extend these measurements to the nonlinear regime by combining phase-shaped FWM imaging with heterodyne detection. We show that high-quality, shaped FWM focal volumes based on a variety of Hermite-Gaussian and Laguerre-Gaussian beam modes can

be obtained. In addition, we demonstrate that the eigenmodes of composite beam shapes such as the Laguerre-Gaussian modes can be selectively visualized.

We use a dual color excitation scheme with incident fields $E(\omega_1)$ and $E(\omega_2)$. The signal is detected at the anti-Stokes shifted frequency $\omega_3 = 2\omega_1 - \omega_2$. Because the signal depends linearly on the ω_2 field, any spatial beam shaping of the ω_2 field will be linearly transferred to the anti-Stokes field.^{4,9} The ω_2 excitation beam is derived from an Nd:YVO₄ mode-locked laser (High-Q laser, 7-ps, 76-MHz rep. rate) and the ω_1 beam from an intra-cavity, frequency-doubled optical parametric oscillator (APE-Levante OPO, 6-ps, 76-MHz rep. rate). The wavelengths of these excitations were fixed at 1064 nm and 815 nm, respectively. The combined excitation beams were sent to an interferometer to generate the local oscillator (LO) field at ω_3 .

The interferometer, shown schematically in Figure 1, includes in one arm a phase-only spatial light modulator (SLM—Holoeye Pluto-NIR) to shape the ω_2 beam profile. The phase curvature of the SLM was corrected to reduce wavefront aberrations.¹⁴ In the other arm of the interferometer, the LO was generated by focusing the incoming beams

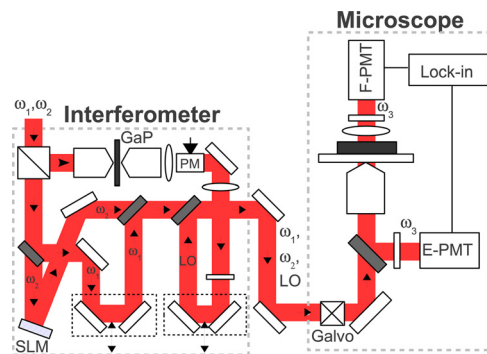


FIG. 1. (Color online) Schematic of the experimental set-up used in the imaging of complex nonlinear excitation profiles in a heterodyne FWM microscope. The interferometer is used to generate the LO, which is combined with the ω_1 and ω_2 excitation beams. The combined beams are sent to the microscope where the four-wave mixing signal interacts with the LO at focus. The PMT signal is fed to the lock-in amplifier to detect the heterodyne signal at 10 MHz modulation.

^{a)}Electronic mail: epotma@uci.edu.

with a 0.66NA microscope objective onto a gallium phosphide (GaP) window. The generated LO radiation was phase modulated using a 10 MHz resonant modulator (PM-Novaphase, EO-PM-R-010). The LO arm also contains a piezo-driven translation stage to vary the optical phase delay between the LO and the excitation beams in the other arm. The three beams were subsequently directed to the microscope using silver mirrors, reflected by galvanometric mirrors and focused with a 1.2NA, water immersion objective lens onto the sample. The FWM signal generated by the sample was detected either in the forward or epi-direction using a photomultiplier tube (PMT) with 650 ± 40 nm band pass filters and fed to a lock-in amplifier, which is synchronized to the 10 MHz modulation. For epi-detection, a 50:50 beam splitter window was used to direct the heterodyne signal onto the PMT.

Silicon nanoparticles (30 nm size, Meliorum Technologies, Inc.) dispersed on a coverslip were used as FWM probes. Figure 2(a) shows the FWM intensity signal from the nanoparticles, which are much smaller than the focal volume and thus provide a non-convolved image of the FWM focal volume. Programming a spatially uniform phase onto the SLM to generate an HG_{00} beam profile (at ω_2), a Gaussian-like FWM focal intensity is obtained. The fringe visibility of the interference between the LO and the FWM radiation, illustrated in Figure 2(b), was measured to be $\sim 60\%$, limited by the overlap between the point-like FWM emission pattern from the nanoparticle and the Gaussian-shaped LO excitation. Figures 2(c) and 2(d) show the in-phase and quadrature FWM images of the silicon nanoparticle, respectively. The FWM signal from glass, which is purely real, was used as a reference for the in-phase and quadrature response from the nanoparticle. Note that the particle's in-phase response is 180° out-of-phase with that of glass and the quadrature electronic response is non-zero. These observations can be attrib-

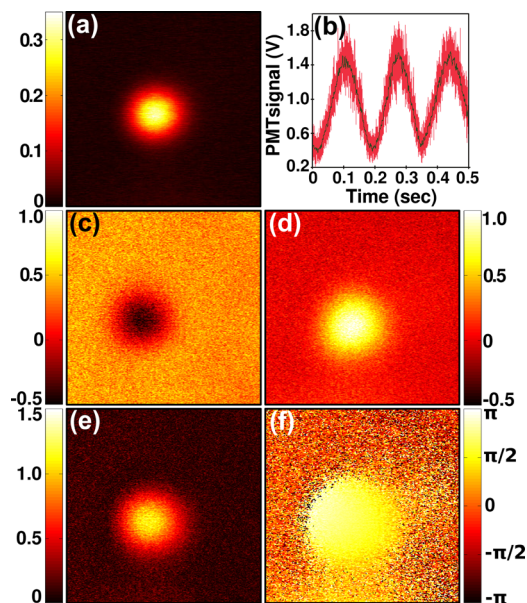


FIG. 2. (Color online) FWM images with HG_{00} input fields. (a) FWM intensity image, (b) Interference between FWM and LO as function of piezo sweep time, (c) in-phase, (d) quadrature phase component of the FWM signal—referenced to glass slide. (e) and (f) are the amplitude and phase profiles calculated from images (c) and (d). The image area is $2.1 \times 2.1 \mu\text{m}$.

uted to the excitation energies being larger than the absorption bandgap of silicon ($\lambda < 1.1 \mu\text{m}$). Figures 2(e) and 2(f) show the amplitude and phase response calculated from the in-phase and quadrature images. The spatial phase shows a slight amount of non-uniformity across the focal plane due to small phase differences in the LO beam relative to the excitation signal.

Next, we shaped the ω_2 spatial profile with HG_{10} and HG_{01} phase patterns by programming the SLM panel into $0-\pi$ phase halves in the horizontal and vertical dimensions, respectively.⁴ Figures 3(a) and 3(c) show the FWM focal intensities for the HG_{10} and HG_{01} beam profiles. The FWM excitation field at focus clearly shows the two-lobed profile along the horizontal and vertical directions. The heterodyne FWM images obtained from the lock-in signal are shown in Figures 3(b) and 3(d), respectively. The inset to these figures shows one-dimensional line scans, which illustrates that the interference signal follows the FWM intensity profiles and accrues a $0-\pi$ phase jump at the center of the excitation profile. We note that in the phase-resolved FWM images of such beam shapes, the zero crossing of the spatial phase in focus is precisely defined and corresponds to the location of the particle. Hence, using the spatial phase, the location of the particle can be accurately determined, which may have interesting implications for particle localization techniques without the need for curve fitting.

We further examined the Laguerre-Gaussian (LG_{01}) beam mode, which is created by applying a vortex phase sweep function on the SLM panel (Figure 4(a)). The FWM focal intensity obtained with the LG_{01} beam shape is given in Figure 4(b), showing the well-known donut profile. Figures 4(c) and 4(d) depict the in-phase and quadrature response, respectively. For these measurements, a reference point is chosen on the donut segment of the intensity image to determine the relative in-phase and quadrature contributions. The in-phase and quadrature responses resemble the HG_{10} and HG_{01} profiles because the LG_{01} mode can be decomposed into HG beam modes as $LG_{01} = HG_{10} + i HG_{01}$. The reconstructed amplitude and phase profiles are given in Figures 4(e) and 4(f). These images clearly

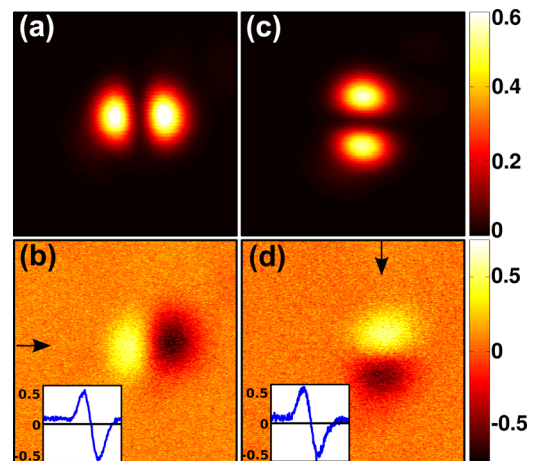


FIG. 3. (Color online) FWM images with HG_{10} and HG_{01} shaped input field at ω_2 . (a),(b) FWM intensity images. (c),(d) heterodyne FWM images—referenced to the peak of the intensity profile. The inset to figures (c) and (d) shows the line scan at locations indicated by the arrows. The image area is $2.1 \times 2.1 \mu\text{m}$.

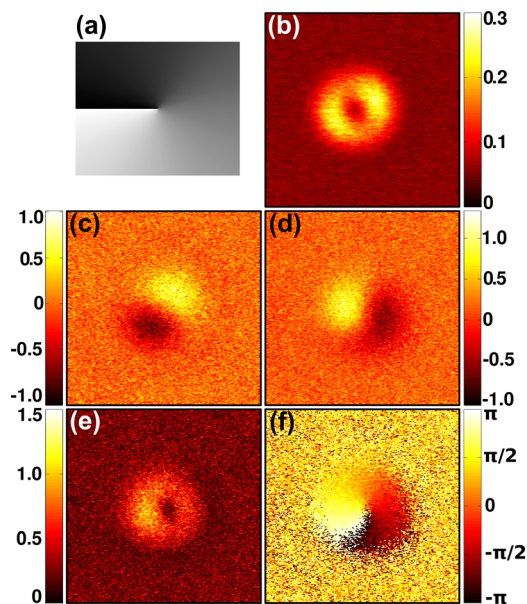


FIG. 4. (Color online) FWM images with LG_{01} shaped input field at ω_2 . (a) SLM phase mask profile showing the vortex phase sweep used to generate the LG_{01} shaped input, (b) FWM intensity image, (c) in-phase, and (d) quadrature phase components of the FWM signal—referenced to a point on the donut intensity profile. (e),(f) are the amplitude and phase profiles calculated from images (c) and (d). The image area is $2.1 \times 2.1 \mu\text{m}$.

demonstrate the vortex phase profile of the tightly focused LG_{01} -shaped field. The ability to image the complex nonlinear excitation fields at the focus allows the visualization of individual eigenmode components of composite beam patterns, which are lost in pure intensity imaging.

In conclusion, we have characterized the amplitude and phase of nonlinear excitation fields in a FWM microscope by combining the heterodyne detection scheme with SLM-based spatial phase shaping. Our results indicate that tightly focused, nonlinear excitation volumes shaped with Hermite-Gaussian and Laguerre-Gaussian beam modes can be synthesized with precisely defined amplitude and phase profiles. While we have focused on the complex nonlinear response in the focal plane only, this technique can be easily extended to map the entire 3D focal excitation volume.

This work is supported by National Science Foundation (NSF) Grant No. CHE-0847097.

¹M. Dyba and S. W. Hell, *Phys. Rev. Lett.* **88**, 163901 (2002).

²A. M. Yao and M. J. Padgett, *Adv. Opt. Photon.* **3**, 161 (2011).

³N. Hayazawa, Y. Saito, and S. Kawata, *Appl. Phys. Lett.* **85**, 6239 (2004).

⁴V. V. Krishnamachari and E. O. Potma, *J. Opt. Soc. Am. A* **24**, 1138 (2007).

⁵N. Oliver and E. Beaurepaire, *Opt. Express* **16**, 14703 (2008).

⁶O. Masihzadeh, P. Schlup, and R. A. Bartels, *Opt. Lett.* **34**, 1240 (2009).

⁷J. Liu, F. Lu, W. Zheng, and Z. Huang, *Appl. Phys. Lett.* **97**, 083701 (2010).

⁸M. R. Beverluis and S. J. Stranick, *Appl. Phys. Lett.* **92**, 231115 (2008).

⁹V. Raghunathan and E. O. Potma, *J. Opt. Soc. Am. A* **27**, 2365 (2010).

¹⁰R. Juskaitis and T. Wilson, *J. Microsc.* **189**, 8 (1998).

¹¹J. N. Walford, K. A. Nugent, A. Roberts, and R. E. Scholten, *Opt. Lett.* **27**, 345 (2002).

¹²F. Charrière, A. Marian, T. Colomb, P. Marquet, and C. Depeursinge, *Opt. Lett.* **32**, 2456 (2007).

¹³M. Muller, A. H. Buist, G. J. Brakenhoff, and J. Squier, *Opt. Commun.* **138**, 16 (1997).

¹⁴C. Li, M. Xia, Q. Mu, B. Jiang, L. Xuan, and Z. Cao, *Opt. Express* **17**, 10774 (2009).